Morphological Changes in Thermoplastic Polyurethanes during Heating

P. R. Laity,[1] J. E. Taylor,[1] S. S. Wong,[2] P. Khunkamchoo,[2] M. Cable,[3] G. T. Andrews,[3] A. F. Johnson,[2] R. E. Cameron[1]

[1]*Materials Science and Metallurgy, University of Cambridge, New Museums Site, Cambridge CB2 3QZ, United Kingdom*
[2]*IRC in Polymer Science and Technology, School of Chemistry, University of Leeds, Leeds LS2 9JT, United Kingdom*
[3]*Ranier Technology Ltd., Greenhouse Park Innovation Centre, Newmarket Rd. Cambridge, CB1 5AS, United Kingdom*

Received 29 March 2005; accepted 15 July 2005
DOI 10.1002/app.22644
Published online in Wiley InterScience (www.interscience.wiley.com).

ABSTRACT: This work investigated the thermal behavior of a series of thermoplastic poly(ether-urethane)s containing 36–71% by weight hard segments derived from 4,4′-methylene-bisphenylisocyanate and butane-1,4-diol, with poly(tetramethylene oxide) soft segments. In all materials studied, differential scanning calorimetry revealed the presence of a T_1 endotherm ~20–30°C above the annealing temperature. Morphological changes during heating were observed using small-angle X-ray scattering; the data was analyzed using "globular" models based on a one-dimensional statistical lattice or the Percus–Yevick description of liquids, both of which appeared to provide good descriptions of these materials. The results indicated that the T_1 endotherm coincided with the onset of morphological changes during heating. Possible explanations are discussed, based on the melting of small hard-segment crystals or an activation energy associated with transient segmental mixing. © 2006 Wiley Periodicals, Inc. J Appl Polym Sci 100: 779–790, 2006

Key words: polyurethane; calorimetry; X-ray scattering; morphology

INTRODUCTION

Thermoplastic polyurethanes (TPUs) are segmented copolymers, composed of multiple "hard" urethane-containing blocks interspersed with more flexible "soft" chain segments.[1–4] Immiscibility of these "hard" and "soft" segments (HS and SS) favor microphase separation, which can occur under suitable processing conditions. The resulting glassy or semicrystalline HS microdomains act as filler and provide physical crosslinks between SS, which are in a rubbery state under normal conditions of use. Hence, TPUs are generally elastomers. In contrast to conventional, chemically-crosslinked rubbers, however, the physical crosslinks in TPUs can be melted, allowing these materials to be melt-processed at elevated temperatures. This facilitates various manufacturing methods, and consequently, TPUs are used in many diverse applications.

Correspondence to: P. R. Laity (petelaity@aol.com).
Contract grant sponsors: Ranier Technology Ltd., DTI, and EPSRC.

Thermal behavior of polyurethanes

The complex thermal behavior of TPUs is well known and has been the subject of numerous publications by Cooper and coworkers,[5–9] Koberstein and coworkers,[10–17] Pascault and coworkers,[18–20] Martin et al.[21–24] and others.[25–34] Differential scanning calorimetry (DSC) often reveals several features between −150 and 250°C, which can be attributed to physical changes within the microphase-separated domains, as well as enthalpy changes associated with segmental mixing and demixing. Composition and processing history have marked effects on the thermal behavior of these materials, although the exact nature of the relationships may not be fully understood.

The glass transition for SS microdomains (T_{gSS}) is generally well below room temperature. For example, T_{gSS} for pure poly(tetramethylene oxide) (PTMO) is reported as −92.8°C[20] to −96°C.[24] In practice, however, TPUs often exhibit a T_g somewhat higher than that expected for pure SS microdomains,[5,6,8,11,12,16,17,20,21,24,33] which may be attributed to incomplete segmental demixing and residual HS dissolved in SS microdomains. Conversely, the HS glass transition for HS microdomains (T_{gHS}) normally occurs well above room temperature. For pure HS based on 4,4′-methylene-bisphenylisocyanate (MDI) and butane-1,4-diol (BDO), T_{gHS} has been reported in the region of 107–110°C.[19,26,35] In this case, however,

residual SS dissolved in HS microdomains is expected to decrease T_g.[6,11,12,21,23,26]

Some SS are prone to crystallization, which results in a melting peak (T_{mSS}) around room temperature.[8,33,34–37] Van Bogart et al.[8] reported that crystallization was more pronounced for higher SS molecular weights and for TPU formulations with lower HS content. This "cold crystallization" is generally regarded as undesirable, since it can cause embrittlement and loss of elastomeric properties at low temperatures.

MDI based TPUs generally exhibit a number of endotherms above 170°C, which can be ascribed to a combination of the microphase mixing transition (T_{MMT}) and melting of hard segment crystals (T_{mHS}). Small-angle X-ray scattering (SAXS) studies of poly(ether urethane)s (PEUs) during heating observed a strong decrease in intensity that coincided with an endotherm in the vicinity of 175°C, which was ascribed to the T_{MMT}.[13–15,32,36] The results of Ryan et al.[36] were particularly significant, since their material was based on BDO and a mixture of 2,4- and 4,4′-MDI isomers, which suppressed HS crystallization and precluded any T_{mHS} peaks. Changes in wide-angle X-ray scattering (WAXS) from polymers based on MDI-BDO between 190 and 230°C have been attributed to T_{mHS}.[12–14] The occurrence of multiple endotherms by DSC may be due to the presence of two polymorphs, as previously noted by Briber and Thomas.[37,38] Koberstein and coworkers[12,13] also noted the possibility of melting the lower temperature form, followed by recrystallization and melting of the higher polymorph.

It appears that different molecular features affect T_{MMT} and T_{mHS}. Consequently, their order can vary between materials, depending on segmental compositions and lengths. Koberstein and coworkers[12–14] found that amorphous HS dissolved into the SS first, and then HS crystals melted and dissolved at higher temperatures. Conversely, a recent study by Saiani et al.[27] suggested that T_{mHS} occurred before T_{MMT}. Significantly, while the PEUs studied by Koberstein and coworkers used MDI + BDO, those studied by Saiani et al. incorporated 2-methyl-1,3-propandiol in the HS, to lower T_{mHS}.

Polyurethanes often show an endotherm (T_1) between 20 and 50°C, above the annealing temperature.[8–11,13,14,22,23,25] The cause of this peak is unclear, at present, although several potential explanations have been suggested. Cooper and coworkers[6,8] attributed T_1 to the loss of short-range order of an unknown nature. Subsequently, Hu and Koberstein[10] suggested that the temperature dependence of T_1 may be linked to the relationship between HS length and solubility, which is embodied in the Koberstein–Stein model of TPU morphology.[39,40] Martin et al.[22] attributed the peak in the temperature range 100–180°C to melting of crystals based on short MDI-BDO sequences. Chen et al.[25] showed that the peak area and temperature both increased with the logarithm of annealing time (log t_a) and ascribed the peak to an enthalpy relaxation. The work reported here provides further insight into the possible morphological origins of the T_1 peak in TPUs.

X-ray scattering is widely used to characterize the structures present in polymers and other materials.[41,42] WAXS is sensitive to the structure on the scale of bond-lengths (typically 0.1–0.2 nm) and can reveal information on crystallinity. SAXS is particularly useful for observing structural features on the scale of the microdomains in segmented copolymers (typically 1–100 nm). Moreover, the intense X-ray illumination available at a synchrotron source permits SAXS and WAXS measurements to be made with acquisition times of a few seconds, so that morphological changes may be observed in "real time" during heating and other experiments. More detailed discussions of X-ray scattering techniques and interpretation of the results can be found elsewhere.[41–44]

Morphological studies using SAXS

A common problem with SAXS studies is that interpretation is seldom unequivocal. Often, several different interpretations of the same data can be made, which may not provide the most accurate or detailed account of the morphology under investigation. If a reliable morphological model can be established (e.g., by electron microscopy or other methods), however, SAXS then provides a convenient method for quantifying the structure (e.g., in terms of distances, volume fractions, or compositions).

It has been demonstrated recently[45–47] that the SAXS patterns from a wide range of TPUs could be interpreted in terms of a "globular" model, of discrete HS microdomains dispersed within a mixed HS + SS phase. According to this model, the observed intensity was proportional to a particle scattering function (P), which depended on the size of the HS microdomains, and a structure factor (S), which described their relative positions:

$$I(q) = I_0 P(q) S(q) \tag{1}$$

I_0 may be regarded as a scaling factor, which depended on the intensity of the incident X-rays, illuminated sample volume, scattering contrast between microphases ($\Delta\rho$) etc, and q was the modulus of the scattering vector:

$$q = \frac{4\pi}{\lambda} \sin\theta \tag{2}$$

where λ was the wavelength and 2θ was the scattering angle. It was found that an adequate expression of the particle scattering function was given by:

$$P(q)=9\left\{\frac{\sin(qR)-qR\cos(qR)}{(qR)^3}\right\}^2 \quad (3)$$

where R was the radius of the scattering bodies. Although this equation was strictly valid only for monodispersed spheres, it appeared to provide a reasonable "first approximation" to scattering from a collection of randomly oriented anisometric bodies.

Two models were found to provide adequate expressions for the structure factor.[45] The simpler expression was based on the one-dimensional statistical lattice model, originally proposed by Zernike and Prins (ZP) to describe WAXS from liquids.[48] In the ZP model

$$S(q)=\frac{1-B^2}{1-2B\cos(qd)+B^2} \quad (4)$$

where d is the average projected distance between scatterers. Assuming a Gaussian distribution of d, with standard deviation σ

$$B=\exp\left\{-\frac{q^2\sigma^2}{2}\right\} \quad (4a)$$

Although better models are now available for the structure of liquids, the ZP model still provides a suitable description of some crystal imperfections.[41,43,44] Moreover, there appears to be no reason why the microphase-separated morphologies of TPUs should be strictly liquid-like.

The second, more complicated expression was based on the Percus–Yevick (PY) model.[49] This appears to provide a more accurate description of liquids[50] and has also been used to describe the microphase-separated morphologies of copolymers.[51,52] According to the PY model

$$S(q)=\left\{1+\frac{24\phi}{x}G(x)\right\}^{-1} \quad (5)$$

where

$$G(x)=\frac{\alpha}{x^2}\{\sin x-x\cos x\}+\frac{\beta}{x^3}\{2x\sin x+(2-x^2)\cos x-2\}+\frac{\gamma}{x^5}\{24-x^4\cos x+(12x^2-24)\cos x+(4x^3-24x)\sin x\} \quad (6)$$

$$\alpha=\frac{(1+2\phi)^2}{(1-\phi)^4} \quad (6a)$$

$$\beta=\frac{-6\phi(1+0.5\phi)^2}{(1-\phi)^4} \quad (6b)$$

$$\gamma=\frac{\phi(1+2\phi)^2}{2(1-\phi)^4}=\frac{\phi}{2}\alpha \quad (6c)$$

ϕ is the volume fraction of scatterers and $x = 2qR_H$. Note that a distinction is made between the particle radius in eq. (3) and the effective "hard sphere" radius (R_H) in eqs. (5) and (6). Commonly, it appears that a "hard shell" boundary layer exists around the microdomains, of thickness h and the same scattering power as the surrounding matrix, which affects their relative positions but does not contribute to the scattering.[46,47,51,52] This can be accommodated using $R_H = R + h$ in eqs. (5) and (6) and scaling ϕ accordingly.

Although these two expression for S are based on somewhat different structural models, the resulting interference functions behave in similar ways.[46,47] Both give series of local maxima, which become broader and lower as q increases, until the functions level off at a value of 1. Consequently, it appeared that the breadth and position of the SAXS peak were dominated by the spatial distribution of microdomains (by way of the interference function), while the tail at high q was controlled by the size of the microdomains. Our previous work[46,47] demonstrated that the observed SAXS from TPUs could be reproduced equally well by either model, although it was felt that the ZP model provided a more intuitive interpretation of the morphological response to deformation.

In the present work, SAXS and WAXS have been used to study the morphological changes in TPUs during heating. This provided a further test of the proposed globular scattering model, while the results also revealed more detailed information concerning the morphological processes underlying the T_1 endotherm observed by DSC.

EXPERIMENTAL

The PEU formulations used in this study incorporated semiaromatic HS derived from MDI and BDO, with PTMO polyether SS. These materials were synthesized using a bulk reaction method, as described previously.[53] The molar ratio of MDI:BDO:macrodiol was maintained at 5 : 4 : 1 and the HS content was controlled through the SS macrodiol molecular weight. Using macrodiols with weight–average molar masses ranging from 650 to 2900 Da, singly or as mixtures, PEU formulations containing 71–36% HS by weight were produced.

Portions of the fully reacted products from the synthesis were hot-pressed between sheets of glass-fiber reinforced PTFE mold release cloth, at 210–220°C, using metal strips as "spacers" to control the thickness. The resulting films were ejected from the press and immediately (i.e., within 10 s) quenched by immersion in iced water, then stored at room temperature until

required. These samples were designated HPQ (i.e., hot-pressed, quenched), although the storage was equivalent to annealing at room temperature (~20°C). Other samples were subsequently annealed at elevated temperatures in a fan-assisted oven.

DSC experiments were performed using a Q1000 thermal analyser (TA Instruments), fitted with a liquid nitrogen cooler. Temperature and heat-flow were calibrated using indium. Samples for DSC measurements (~10 mg) were cut using a punch and sealed into aluminum pans. The samples were automatically loaded into the thermal analyzer at 35°C, and then rapidly cooled to −150°C. The system was allowed to achieve thermal equilibrium, and then measurements were made during heating at 20°C min^{-1}, from −150 to 250°C.

Simultaneous SAXS/WAXS/temperature-rise experiments were performed at the SRS, Daresbury, on experimental stations 8.2 (now closed) and 16.1, using X-ray wavelengths of 0.153 and 0.141 nm, respectively. Samples, in aluminum pans sealed with mica, were loaded into a "Linkam" hot-stage at room temperature, and then heated at 5°C min^{-1}, from 25 to 250°C. SAXS data were collected using a wire "quadrant" detector; WAXS data were collected using an INEL "knife-edge" detector. Each frame of X-ray scattering data was collected over 12 s, such that consecutive frames corresponded to a 1°C temperature rise.

The q-range observable by the SAXS detector was calibrated against the known peak positions from wet rat-tail collagen and the detector response was measured using the "flood-field" from an ^{55}Fe radioactive source. The angular range observable by the WAXS detector was calibrated against the known peak positions of HDPE or triphenylamine.

Raw data were corrected for variations in detector response, incident light intensity, absorption by the sample and background scattering, then converted to comma-separated variable files using the xotoko and reconv2 programs (available from the SRS, Daresbury). The corrected data were analyzed using Microsoft® Excel. Curve-fitting was performed using the "solver" tool,[54] with up to 100 iterations, a precision of 0.000001, a tolerance of 5%, and a convergence of 0.001. The options of tangent estimates, forward derivative, and the Newton search method were used.

RESULTS

DSC data for samples annealed for 24 h at 83°C are shown in Figure 1. The softer formulations exhibited inflections around -70°C, which may be attributed to T_{gSS}. This was roughly 25°C above the T_g reported for pure PTMO, which is consistent with incomplete microphase separation of HS from the SS microdomains in these formulations. Using the linear relationship reported by Chen et al.,[26] the observed T_{gSS} corresponded to about 13% HS dissolved in the SS. The

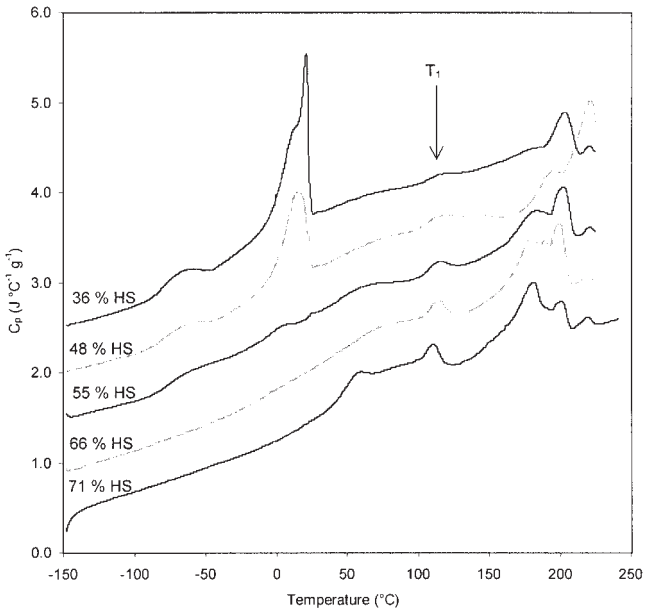

Figure 1 DSC data for TPU formulations with different HS content, after annealing for 24 h at 83°C (curves off-set vertically for ease of viewing).

location of T_{gSS} appeared to be essentially independent of overall TPU formulation, but its magnitude decreased with increasing HS content and it could not be observed in the hardest formulations.

The softest formulations also exhibited a broad endotherm between −10 and 25°C, which may be ascribed to T_{mSS}. It should be noted that this peak occurred below the sample loading temperature into the DSC, which implied that SS crystallization occurred during the analyses. Although the data were not recorded, a large exotherm was usually observed while the samples were being cooled to the starting temperature. Further crystallization during the measurements would also explain the dip between T_{gSS} and T_{mSS}, for the softest materials.

The hardest formulation exhibited an inflection around 50°C, which may be attributed to T_{gHS}. Again, using the linear relationship reported by Chen et al.,[26] this would correspond to roughly 70% HS, which is close to the overall composition of this material. This feature appeared to become broader, starting at lower temperature with increasing SS content, which may indicate increasingly variable composition in the HS microdomains of softer formulations. As a result of the broadening, this feature became progressively more difficult to observe in the softer materials and was further obscured by the strong T_{mSS} endotherm in the softest materials.

The T_1 peak was observable around 115°C, which corresponded to roughly 32°C above the annealing temperature (24 h at 83°C) for the data presented in Figure 1. This endotherm appeared most clearly for

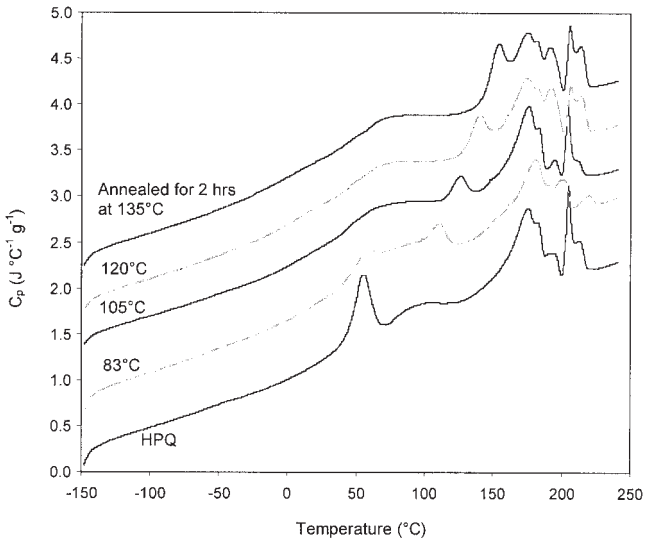

Figure 2 DSC data for 71% HS formulation after different thermal history (curves off-set vertically for ease of viewing).

the hardest formulations, but became broader and less prominent for softer formulations. Moreover, although it can be notoriously difficult to locate the "baseline" in complex DSC traces such as these, the T_1 peaks for the hardest formulations appeared to be followed immediately by small exotherms.

The relationship between T_1 and annealing temperature for samples of the 71% HS formulation is demonstrated in Figures 2 and 3. T_1 appeared to increase linearly with annealing temperature, eventually merging into the multiple high temperature peaks above 170°C, for samples annealed above 135°C. Similar results were also observed for the other formulations studied.

The data for the HPQ samples deserve special mention. The very prominent T_1 peak for these samples appeared to coincide with T_g and was followed by an exotherm that may be attributed to microphase separation. (This is supported by the SAXS data presented below.) The implication is that these materials had been quenched into a glassy, predominantly mixed HS + SS phase, within which the processes responsible for T_1 could still occur.

Finally, all the materials exhibited multiple endothermic peaks above 170°C. These features appeared to depend on both the formulation and thermal history of the samples studied and may be attributed to combinations of T_{MMT} and T_{mHS}.[12–15,32,36]

SAXS data from samples of the 71% HS formulation after various thermal histories are presented in Figure 4, along with fitted curves generated using the globular scattering model. The scattering from the HPQ samples was relatively weak, which suggested that little microphase separation had occurred in this material. By contrast, much stronger scattering, in the form of an "interference" peak, was observed from materials that had been annealed at elevated temperatures (i.e., above T_g of the mixed HS + SS phase). The peak height increased with annealing temperature and moved toward lower q, which suggested an increase in the extent of microphase separation and the characteristic lengths of the resulting morphologies.

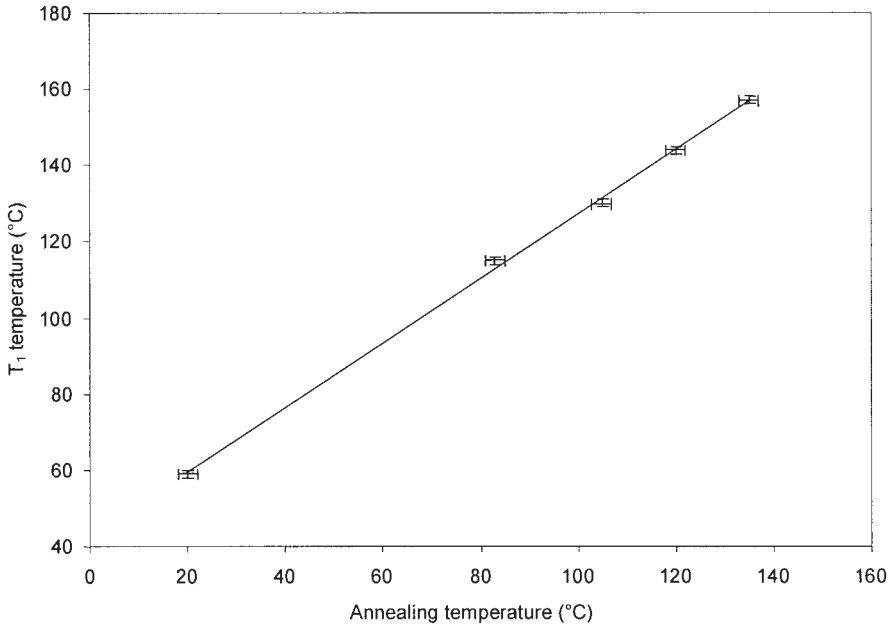

Figure 3 Relationship between annealing temperature and T_1 temperature for 71% HS formulation (error bars indicate uncertainty in T_a and T_1.

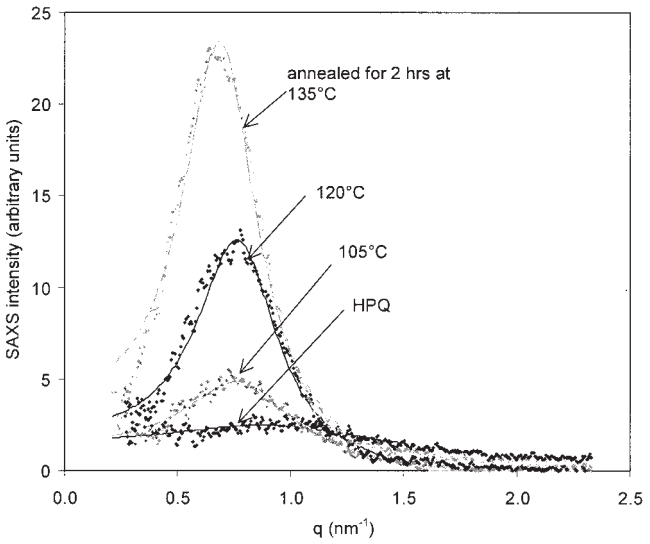

Figure 4 SAXS data for samples of 71% HS formulation after various thermal histories with fitted curves generated using PY model.

The curves in Figure 4 were generated using the PY structure function, although equally good fits were obtained using the ZP model. Some deviation between the model and the data was observed close to the beamstop, which may be attributed to error in background subtraction. Also, the model returned to the baseline on the high-q side of the peak more quickly than did the experimental data and exhibited a series of progressively decreasing "ripples," which can be attributed to the oversimplified assumption of monodispersed scatterers. Nevertheless, the globular scattering model generally fitted the data very well.

Morphological information obtained by curve-fitting is summarized in Table I. Annealing at higher temperatures produced progressively coarser morphologies, in terms of the sizes of and distances between the dispersed scatterers. Although the two versions of the globular scattering model revealed similar trends with increasing annealing temperature, simple geometric calculations using the values of R and d from the ZP model produced higher estimates of ϕ than those given by the PY model. This may be attributed to differences in the probability distributions of interparticle distances. Both versions of the scattering model also indicated that contrast increased with annealing temperature, suggesting larger composition differences between microdomains.

TABLE II
Summary of Morphological Results from Curve-Fitting SAXS Data, for Different TPU Formulations Annealed for 24 h at 83°C

% HS	ϕ	d (nm)	R (nm)	I_0
71	0.055	6.4	2.3	9.3
66	0.059	6.3	2.1	9.0
62	0.045	6.6	2.6	13.2
55	0.032	7.3	2.8	18.0
48	0.010	12.3	3.8	18.8
45	0.027	9.5	3.3	19.2
36	0.017	10.8	3.5	32.4

HPQ samples of the softer TPUs exhibited more microphase separation than did the 71% HS formulation, which may be attributed to lower T_g, for the corresponding mixed HS + SS phases. The scattering contrast increased in the softer formulations, which suggested greater composition differences between microdomains in the materials containing longer SS. Once again, the globular scattering model was able to reproduce the data very well. The results are presented in Table II, for materials annealed for 24 h at 83°C. The trends shown by ϕ and d suggested that the scatterers were dispersed HS microdomains, which were larger in the softer formulations.

Typical SAXS data acquired from a HPQ 71% HS sample during heating is presented in Figure 5, along with model curves based on the globular model. The curves shown were generated using the PY model, although the ZP version produced equally good fits. The data appeared similar to that from samples annealed at different temperatures, shown in Figure 4. The scattering remained relatively weak below 60°C, but increased dramatically above this temperature, which was consistent with the microphase separation exotherm observed by DSC. As the temperature was

TABLE I
Morphological Interpretation of SAXS Data for 71–650 Formulation after Different Thermal Histories

Samples	Zernike–Prins model				Percus–Yevick model			
	d (nm)	R (nm)	σ/d	Scaling factor	ϕ	R (nm)	h (nm)	Scaling factor
HPQ samples	a	a	a	a	a	a	a	a
Annealed samples								
24 h at 85°C	6.7 ± 0.1	2.3 ± 0.1	0.40 ± 0.02	8.9 ± 0.1	0.049 ± 0.002	2.2 ± 0.1	1.4 ± 0.1	7.5 ± 0.1
2 h at 105°C	6.5	2.4	0.34	19.7	0.067	2.2	1.3	16.6
2 h at 120°C	7.2	2.6	0.33	23.9	0.074	2.5	1.3	20.5
2 h at 135°C	7.9	2.8	0.34	43.1	0.064	2.7	1.6	36.3

"a" indicates SAXS data too weak to be analysed reliably.

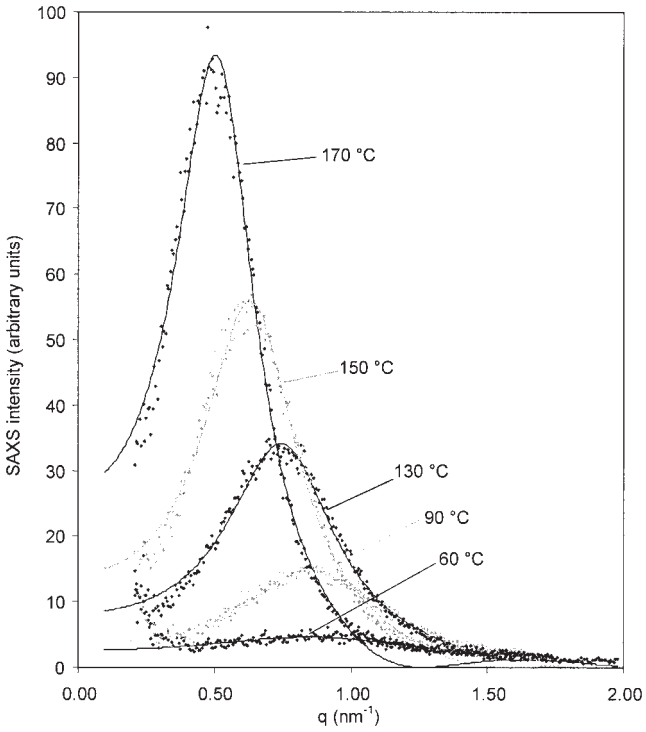

Figure 5 SAXS data measured during heating HPO 71% HS sample, with fitted curves generated using PY model.

raised further, the SAXS peak increased in height and moved toward lower q, eventually merging into the beamstop shadow above 190°C.

Changes in the morphology revealed by curve-fitting SAXS data from HPQ 71% HS samples are presented in Figure 6. The SAXS data below 50°C was too weak to permit reliable curve-fitting. Above this temperature, however, the effective radius of the scatterers (from either model), the average interdomain distance (from ZP), the scaling factor (from either model), and volume fraction (from PY) all increased rapidly, which was consistent with the onset of microphase separation. After this rapid initial development, R, d and I_0 increased more slowly above approximately 70°C, before accelerating again at higher temperatures. By contrast, the increase in ϕ became progressively slower up to ~170°C, then decreased rapidly at higher temperature, consistent with reaching T_{MMT}. The morphological analysis was stopped at 200°C, since the results became less reliable as the interference peak "disappeared" into the beamstop shadow.

Typical SAXS data from an annealed TPU sample (71% HS annealed 2 h at 135°C) is shown in Figure 7, along with fitted curves. Once again, the PY and ZP models gave equally good fits. This data appeared essentially similar to that obtained from HPQ samples, apart from two key features. First, as already demonstrated in Figure 4, microphase separation that had occurred during annealing resulted in significant interference peaks. Second, although the changes observed during heating were qualitatively similar, the temperatures at which they occurred depended on the thermal histories of the samples. In the case of the data presented in Figure 7, the SAXS peak height increased relatively little below 155°C, but considerably faster above this temperature.

It was found that the SAXS data from all the TPU formulations and thermal histories studied here could be fitted well using the globular model, which allowed the morphological changes to be investigated. Selected results for samples of 71% HS TPU with different thermal histories are compared in Figure 8. In each case, it appeared that R and d for the annealed samples remained essentially constant at low temperature, until they intersected the results for HPQ samples and lower annealing temperatures, which occurred at the T_1 temperature observed by DSC. Above T_1, the morphologies suddenly started to change; R and d increased progressively, with each parameter apparently following a single curve at higher temperature, irrespective of annealing temperature.

Moreover, although the starting morphologies depended on both thermal history and composition, all the TPUs investigated exhibited qualitatively similar behavior during heating. This is demonstrated by values of R for the softest formulation used in this study (36% HS), which are presented in Figure 9.

By contrast, clear differences were observed between ϕ and the other morphological parameters. This is demonstrated by the results for the 71% HS formulation, which are presented in Figure 10. Although ϕ remained essentially constant at low temperature, for each of the annealed samples, only the plot for the material annealed at 85°C appeared to intercept the HPQ plot in the vicinity of T_1. Plots for samples annealed at higher temperatures converged with the HPQ results above about 160°C, when ϕ started to decrease in the vicinity of T_{MMT}. Moreover, no clear hierarchy based on annealing temperature was found; the highest starting values of ϕ were observed for the samples annealed at 120°C, while the results for the samples annealed at 105 and 135°C appeared to be essentially identical.

It should also be noted that the estimates of ϕ based on curve-fitting exhibited similar trends to the scattering invariant:

$$Q = 4\pi \int_0^\infty q^2 I(q) dq \tag{7}$$

$$= V(\Delta\rho)^2 \phi(1-\phi) \tag{7a}$$

which is independent of the precise morphology, but depends directly on the volume fractions and scatter-

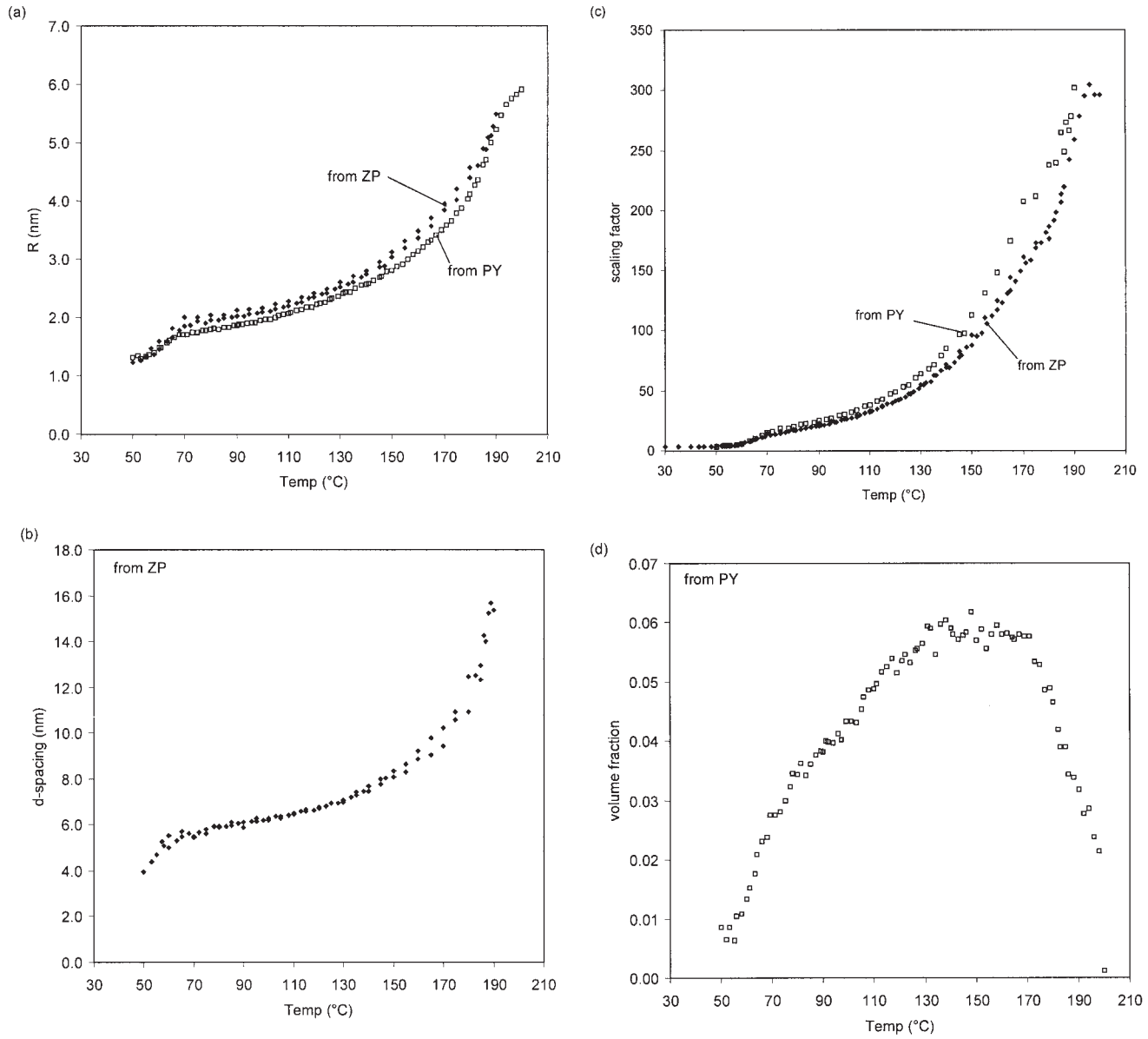

Figure 6 Morphological changes during heating HPQ 71% HS samples, obtained by curve-fitting SAXS data. (a) Effective radius of HS microdomains, (b) interdomain spacing, (c) scaling factor, (d) volume fraction (experiments performed in duplicate).

ing contrast between microdomains.[41,42] This is demonstrated in Figure 11.

Typical examples of the WAXS data collected from 71% HS and 36% HS TPU formulations during heating are presented in Figure 12. Harder formulations exhibited a single broad peak between ~12 and 30° (as shown in Fig. 12(a)), which may be attributed to scattering from noncrystalline HS and SS. This peak appeared to move to lower angle as the temperature was raised, which may be attributed to thermal expansion affecting the radial distribution function. There was, however, no evidence of crystallinity in any of the harder formulations studied.

The softer formulations exhibited sharp crystalline peaks (at ~18.2 and 22.0°) at the start of the heating experiments, which can be attributed to SS crystallinity. These peaks diminished rapidly between 35 and 40°C, which was essentially consistent with the observations of T_{mSS} by DSC. The slightly lower T_{mSS} observed by DSC may be attributed to differences in the crystallite sizes resulting from the thermal histories; samples for X-ray scattering were loaded below 25°C and would retain most of the SS crystallinity developed during storage, whereas the DSC samples were loaded between 35 and 40°C, and so only crystals formed during the cooling and low temperature stages of the measurements would contribute to the T_{mSS} endotherm. Only the broad, amorphous background scattering remained above 40°C, moving progressively toward lower q as the temperature was raised.

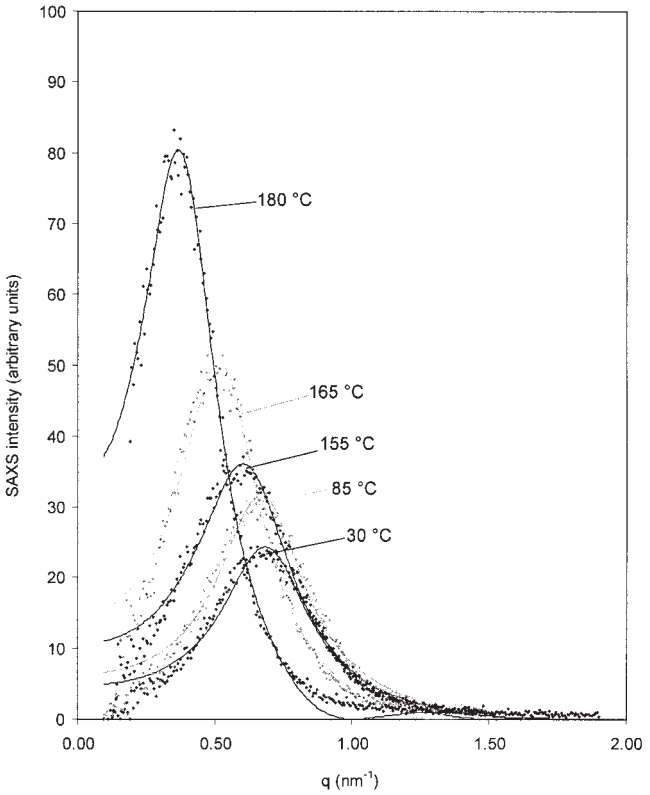

Figure 7 SAXS data measured during heating 71% HS sample annealed 2 h at 135°C with fitted curves generated using PY model.

DISCUSSION

It was reported previously[46,47] that the globular model provided a good description of the SAXS patterns exhibited by some TPUs and their underlying morphological behavior during uniaxial extension. The work presented here indicated that this model was also able to provide plausible explanations for the changes in SAXS patterns for TPUs during heating.

The results indicated small volume fractions of dispersed HS microdomains in the materials studied, even for relatively hard formulations. This rather limited extent of microphase separation, compared with the mass fractions of HS and SS in the formulations used, may appear somewhat surprising. As noted previously,[46,47] however, the potential for weak but numerous interactions between HS urethane and SS ether groups may promote a degree of miscibility. Moreover, the materials used in this and the previous work had relatively short average HS lengths, which is also expected to favor segmental mixing. Hence, while the globular model appeared suitable for these materials, it may be inappropriate for other TPUs exhibiting stronger microphase separation, either as a result of segment length or chemical composition.

Both versions of the globular scattering model, incorporating the structure factors based on ZP or PY models, fitted the SAXS data equally well. It was found, however, that simple geometric calculations based on the values of R and d from the ZP model indicated larger ϕ than what was estimated by the PY model. This may be attributed to differences in the probability distributions of interparticle distances embodied in the models. Deliberately broadening the distribution in the ZP model resulted in lower estimates of d. Moreover, decreasing the boundary layer thickness around the scatterers, which affected the distribution of interparticle distances in the PY model, produced higher estimates of ϕ. As noted previously, there appears to be no reason why the dispersed mi-

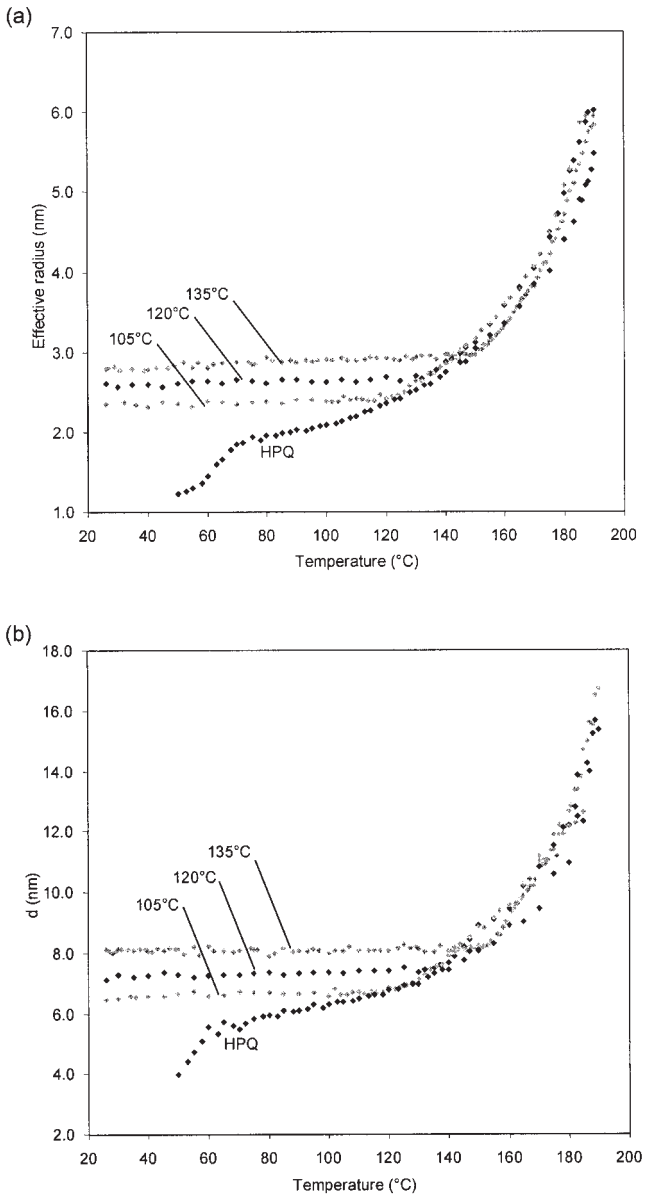

Figure 8 Morphological changes (from ZP model) during heating for HPQ 7I% HS samples and after annealing for 2 h at temperatures shown: (a) effective radius of HS microdomains, (b) interdomain spacing.

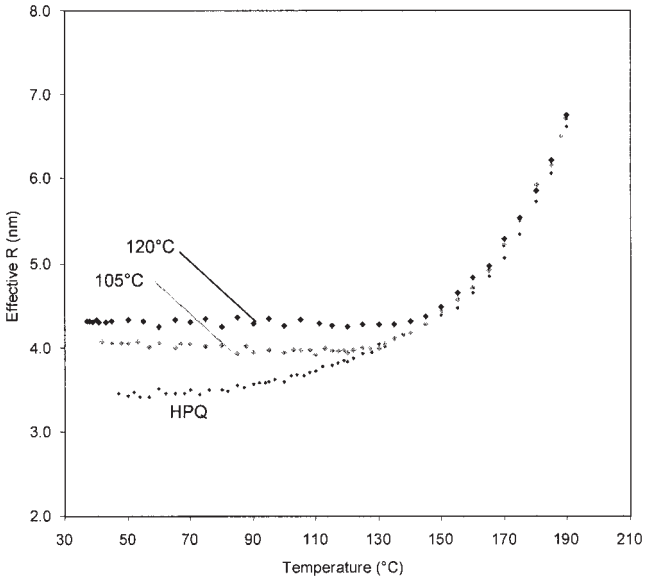

Figure 9 Changes in effective radius of HS microdomains during heating, for HPQ 36% HS samples and after annealing for 2 h at temperatures shown.

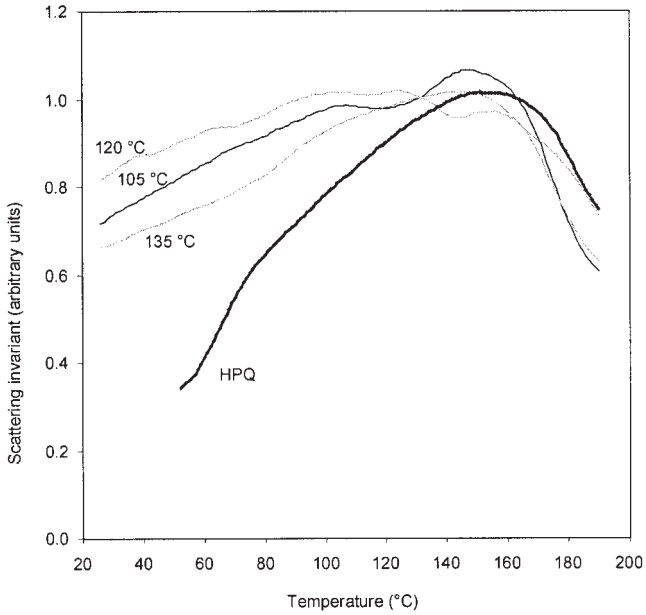

Figure 11 Scattering invariant for HPQ 71% HS samples and after annealing for 2 h at temperatures shown.

crodomains in TPUs should exhibit liquid-like distributions, as embodied in the PY model, nor Gaussian distributions of *d*-spacings, as assumed in the ZP model. Consequently, while the general morphological behavior revealed by this SAXS analysis appears plausible, an overly quantitative interpretation of the results should be avoided.

Analysis of the SAXS data indicated strong correlations between the onset of morphological changes during heating and T_1 observed by DSC. A progressive coarsening of the morphology was generally observed, in terms of the size of dispersed microdomains, the interdomain spacings, and the scattering contrast. Changes in morphology associated with the onset of T_{MMT} have been reported previously[15,32,36]; however, the present work appears to provide the first evidence for changes in morphology at T_1. And, although this did not prove a direct causal link, these observations suggested two possible explanations for the T_1 endotherm.

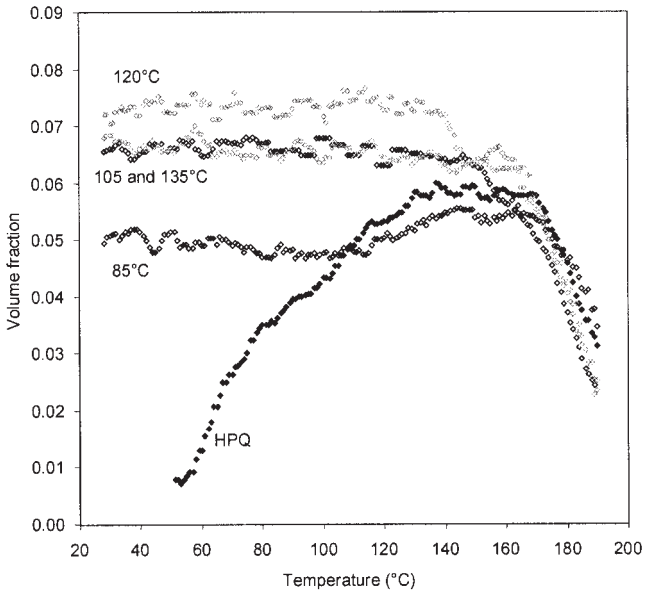

Figure 10 Changes in volume fraction for HPQ 71% HS samples and after annealing for 2 h at temperatures shown.

The driving force for the morphological changes can be attributed to the reduction of less favorable heterogeneous contacts between HS and SS, which may be associated with the interfacial area between microdomains and incomplete segmental demixing within microdomains. This is demonstrated with respect to the behavior of the 71% HS formulation annealed at 105°C, in Figure 13. The relative interfacial area was estimated as:

$$A = \frac{3\phi}{R} \tag{8}$$

assuming the dispersed microdomains to be roughly spherical. This remained essentially constant at low temperature, but decreased rapidly above T_1, by a process that appeared similar to "Ostwald ripening." At the same time, the progressive increase in I_0 above T_1 was consistent with growing composition differences between microphases, due to improved segmental demixing. By contrast, the overall volume fraction of the dispersed microdomains remained effectively constant up to T_{MMT}, around 170°C.

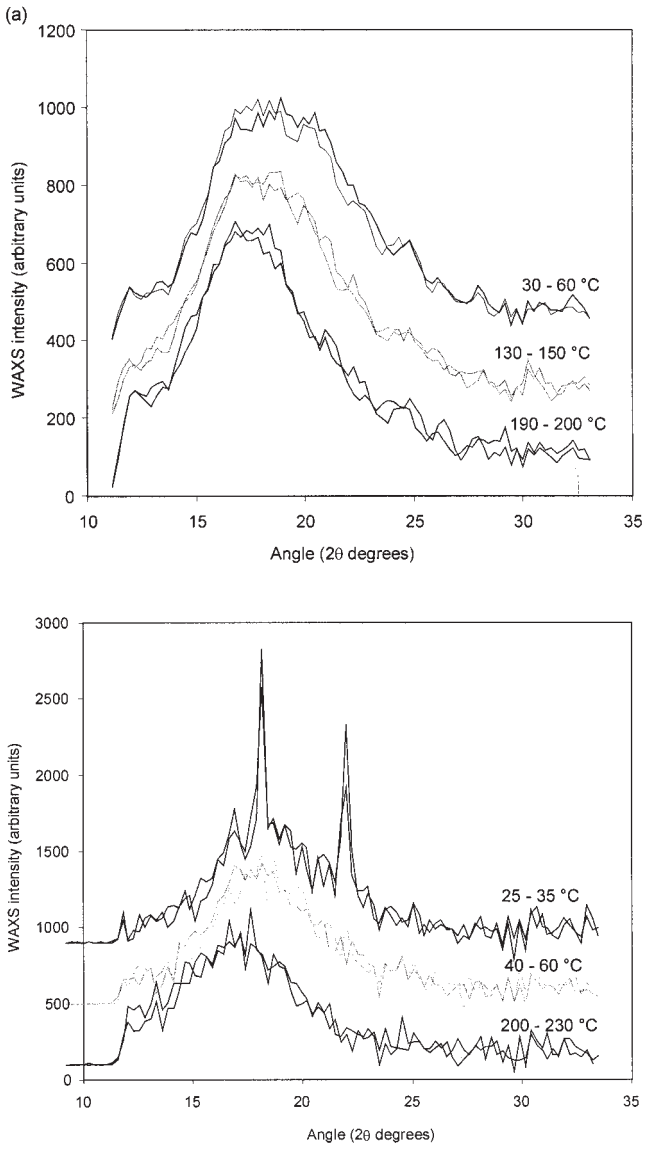

Figure 12 WAXS data measured during heating for (a) 71% HS sample annealed 2 h at 135°C; (b) 36% HS sample annealed 2 h at 120°C (data in duplicate for the temperature ranges shown, curves off-set vertically for ease of viewing).

It has been suggested previously that the T_1 endotherm was due to the melting of small or imperfect HS crystals.[22] Certainly, the increase in HS motion associated with melting could be consistent with the observed onset of further morphological developments, while the severe constraints on volume fraction and peak broadening due to the small crystal size (i.e., no larger than the HS microdomains, $R < 4$ nm) would explain the lack of observable crystalline WAXS peaks.

Since the polymer chains in the TPUs are expected to be highly entangled, the morphological changes observed above T_1 must involve reptation, as described by the Doi–Edwards model.[55] Hence, as an alternative explanation, the T_1 endotherm may represent the activation energy for this process. Several authors[56,57] have noted that "long-range" reptation of segmented copolymers must involve transient segmental mixing. In their original publication, Bouchaud and Cates[56] argued that reptation would be strongly impeded by the resulting periodic potential, for even relatively small positive values of the interaction parameter and segment lengths greater than the entanglement length. Subsequently, Semenov[57] proposed that reptation would be slowed but not completely stopped, since short sections of chains could move independently as a result of short-range Rouse modes.

Moreover, these explanations are not mutually exclusive. The "transient segmental mixing" hypothesis could explain the apparent T_1 endotherm prior to microphase separation in the HPQ 71% HS material and provide a mechanism for initiating microdomain formation. HS crystallization would increase the energy penalty associated with transient segmental mixing, giving a stronger impediment to reptation.

CONCLUSIONS

The work reported here provided further support for a "globular model" interpretation of the morphology exhibited by PEUs with HS based on MDI + BDO. This interpretation implied relatively small volume fractions of dispersed HS microdomains, resulting from incomplete segmental demixing. However, since this may be due to partial miscibility between the HS and SS of the materials studied, the "globular model" may be inappropriate for other more strongly microphase-separated TPUs.

The results demonstrated an apparent link between T_1 and the onset of morphological changes in the TPUs. Hence, the T_1 endotherm appeared to represent the activation energy for the underlying dynamic pro-

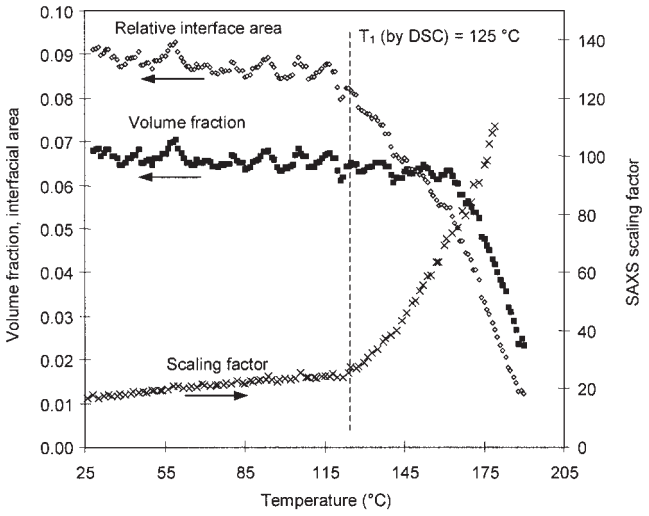

Figure 13 Volume fraction and estimated interfacial area for 71% HS samples after annealing for 2 h at 105°C.

cesses, which may be associated with the melting of small HS crystals or transient segmental mixing.

The help of N. Terrill and A. Gleeson in setting up stations 8.2 and 16.1 at the SRS is gratefully acknowledged. The authors especially thank S. Freeburn, K. Noorsal, and A. Renouf, who helped to perform the experiments on which this paper is based.

References

1. Wirpsza, Z. Polyurethanes: Chemistry, Technology and Applications; Ellis Horwood: Chichester, 1993.
2. Hepburn, C. Polyurethane Elastomers, 2nd ed.; Elsevier Science: Barking, 1992.
3. Woods, G. The ICI Polyurethanes Book, 2nd ed.; ICI Polyurethanes: Everberg, 1990.
4. Abouzahr, S.; Wilkes, G. L. In Processing, Structure and Properties of Block Copolymers; Folkes, M. J., Ed.; Elsevier Applied Science: London, 1985; Chapter 5.
5. Valenkar, S.; Cooper, S. L. Macromolecules 2000, 33, 382.
6. Valenkar, S.; Cooper, S. L. Macromolecules 1998, 31, 9181.
7. Speckhard, T. A.; Gibson, P. E.; Cooper, S. L.; Chang, V. S. C.; Kennedy, J. P. Polymer 1985, 26, 55.
8. Van Bogart, J. W. C.; Bluemke, D. A.; Cooper, S. L. Polymer 1981, 22, 1428.
9. Seymour, R. W.; Cooper, S. L. Macromolecules 1973, 6, 48.
10. Hu, W.; Koberstein, J. T. J Polym Sci Polym Phys Ed 1994, 32, 437.
11. Koberstein, J. T.; Leung, L. M. Macromolecules 1992, 25, 6205.
12. Koberstein, J. T.; Galambos, A. F.; Leung, L. M. Macromolecules 1992, 25, 6195.
13. Koberstein, J. T.; Galambos, A. F. Macromolecules 1992, 25, 5618.
14. Galambos, A. F.; Russell, T. R.; Koberstein, J. T. Polym Mater Sci Eng 1989, 61, 359.
15. Koberstein, J. T.; Russell, T. P. Macromolecules 1986, 19, 714.
16. Leung, L. M.; Koberstein, J. T. Macromolecules 1986, 19, 706.
17. Leung, L. M.; Koberstein, J. T. J Polym Sci Polym Phys Ed 1985, 23, 1883.
18. Etienne, S.; Vigier, G.; Cuvé, L.; Pascault, J. P. Polymer 1994, 35, 2737.
19. Cuvé, L.; Pascault, J. P.; Boiteux, G.; Seytre, G. Polymer 1991, 32, 343.
20. Camberlin, Y.; Pascault, J. P. J Polym Sci Polym Chem Ed 1983, 21, 415.
21. Martin, D. J.; Meijs, G. F.; Gunatillake, P. A.; Yozghatlian, S. P.; Renwick, G. M. J Appl Polym Sci 1999, 71, 937.
22. Martin, D. J.; Meijs, G. F.; Gunatillake, P. A.; McCarthy, S. J.; Renwick, G. M. J Appl Polym Sci 1997, 64, 803.
23. Martin, D. J.; Meijs, G. F.; Renwick, G. M.; McCarthy, S. J.; Gunatillake, P. A. J Appl Polym Sci 1996, 62, 1377.
24. Martin, D. J.; Meijs, G. F.; Renwick, G. M.; McCarthy, S. J.; Gunatillake, P. A. J Appl Polym Sci 1996, 62, 557.
25. Chen, T. K.; Shieh, T. S.; Chui, J. Y. Macromolecules 1998, 31, 1312.
26. Chen, T. K.; Chui, J. Y.; Shieh, T. S. Macromolecules 1997, 30, 5068.
27. Saiani, A.; Daunch, W. A.; Verbeke, H.; Leenslag, J.-W.; Higgins, J. S. Macromolecules 2001, 34, 9059.
28. Eisenbach, C. D.; Stadler, E. Macromol Chem Phys 1995, 196, 1981.
29. Eisenbach, C. D.; Heinemann, T. Macromol Chem Phys 1995, 196, 2669.
30. Frontini, P. M.; Rink, M.; Pavan, A. J Appl Polym Sci 1993, 48, 2023.
31. Frontini, P. M.; Rink, M.; Pavan, A. J Appl Polym Sci 1993, 48, 2003.
32. Li, Y.; Gao, T.; Liu, J.; Linliu, K.; Desper, C. R.; Chu, B. Macromolecules 1992, 25, 7365.
33. Lee, D.-K.; Tsai, H.-B. J Appl Polym Sci 2000, 75, 167.
34. Chen, K. S.; Yu, T.-L.; Tseng, Y.-H. J Polym Sci Polym Chem Ed 1999, 37, 2095.
35. MacKnight, W. J.; Yang, M.; Kajiyama, T. Polym Prepr (Am Chem Soc Div Polym Chem) 1968, 9, 860.
36. Ryan, A. J.; Macosko, C. W.; Bras, W. Macromolecules 1992, 25, 6277.
37. Briber, R. M.; Thomas, E. L. J Polym Sci Polym Phys Ed 1985, 23, 1915.
38. Briber, R. M.; Thomas, E. L. J Macromol Sci Phys 1983, B22, 509.
39. Koberstein, J. T.; Stein, R. S. J Polym Sci Polym Phys Ed 1983, 21, 2181.
40. Koberstein, J. T.; Stein, R. S. J Polym Sci Polym Phys Ed 1983, 21, 1439.
41. Roe, R.-J. Methods of X-Ray and Neutron Scattering in Polymer Science; Oxford University Press: New York, 2000.
42. Glatter, O.; Kratky, O. Small-Angle X-Ray Scattering; Academic Press: London, 1982.
43. Guinier, A. X-Ray Diffraction in Crystals, Imperfect Crystals and Amorphous Bodies; Dover: New York, 1994.
44. Hosemann, R.; Bagchi, S. N. Direct Analysis of Diffraction by Matter; North-Holland: Amsterdam, 1962.
45. Blundell, D. J.; Eekhaut, G.; Fuller, W.; Mahendrasingam, A.; Martin, C. Polymer 2002, 43, 5197.
46. Laity, P. R.; Taylor, J. E.; Wong, S. S.; Khunkamchoo, P.; Norris, K.; Cable, M.; Andrews, G. T.; Johnson A. F.; Cameron, R. E. Polymer 2004, 45, 7273.
47. Laity, P. R.; Taylor, J. E.; Wong, S. S.; Khunkamchoo, P.; Norris, K.; Cable, M.; Andrews, G. T.; Johnson, A. F.; Cameron, R. E. Polymer 2004, 45, 5215.
48. Zernike, F.; Prins, J. A. Z Phys 1927, 41, 184.
49. Percus, J. K.; Yevick, G. J. Phys Rev 1958, 110, 1.
50. Cusack, N. E. The Physics of Structurally Disordered Matter; Adam Hilger: Bristol, 1987.
51. Kinning, D. J.; Thomas, E. L. Macromolecules 1984, 17, 1712.
52. Krakovský, I.; Bubeníková, Z.; Urakawa, H.; Kajiwara, K. Polymer 1997, 38, 3637.
53. Laity, P. R.; Taylor, J. E.; Wong, S. S.; Khunkamchoo, P.; Norris, K.; Cable, M.; Chohan, V.; Andrews, G. T.; Johnson, A. F.; Cameron, R. E. J Macromol Sci Phys 2004, B43, 95.
54. Ivens, K.; Carlberg, C.; Padwick, G.; Honeycutt, J.; Rahmel, D.; Pagan, K. D.; Fuller, S.; Warner, S.; Warner, N.; Karlins, D.; Voss, R.; Person, R. Using Microsoft® Office® 97; Que Corp: Indianapolis, 1997.
55. Doi, M.; Edwards, S. F. The Theory of Polymer Dynamics; Clarendon Press: Oxford, 1986.
56. Bouchaud, J. P.; Cates, M. E. J Phys II France 1993, 3, 1171.
57. Semenov, A. N. Phys Rev E 1999, 60, 3076.